Journal of Applied Mechanics and Technical Physics, Vol. 42, No. 6, pp. 929–941, 2001

SIMULATION OF THE MOTION AND HEATING OF AN IRREGULAR PLASMA

V. T. Astrelin,[1] A. V. Burdakov,[1] N. A. Huber,[2] and V. M. Kovenya[3]

UDC 517.958:537.84

A physicomathematical model for plasma heating and confinement is formulated on the basis of some assumptions on the behavior of a dense plasma cloud in a magnetic field. The model allows for the ionization and heating of the plasma cloud by the surrounding deuterium plasma due to heat conduction and heating by a superthermal electron current. The expansion of a plasma cloud in an external magnetic field is studied using some simplifications in a magnetohydrodynamic approximation. Plasma heating is modeled by an external source. The basic equations include continuity, motion, energy, and magnetic-field equations. For numerical solution of the problem, we developed a finite-difference scheme of the type of a universal algorithm with splitting into physical processes and spatial directions, which allowed us to obtain separate solutions of the equations of magnetic induction and gas dynamics. Calculations of the propagation of a plasma cloud heated by a source in an external magnetic field were performed. The mechanism of the effect of the magnetic field and heat source on plasma cloud expansion is determined. The results agree qualitatively with experimental data.

INTRODUCTION

In recent decades, plasma heating and confinement has become an important problem in plasma physics. Because of the variety of regimes, the wide range of parameters of the medium, and the complexity and nonlinearity of the examined processes, problem of plasma heating and propagation is a multiparameter one, which requires using various approaches to solve it. In the present work, we attempted a numerical simulation of the plasma dynamics under conditions corresponding to the experiment performed on the GOL-3 facility at the Institute of Nuclear Physics of the Siberian Division of the Russian Academy of Sciences. This facility is used in experiments on formation and heating of a dense gas cloud originating from a grain (target) of lithium deuteride or another material that vaporizes under the action of a powerful relativistic electron beam (REB) and interacts with the background plasma [1]. It should be noted that simulations of plasma heating and dynamics on the GOL-3 facility have also been performed earlier but the plasma was studied without a target within the framework of a one-dimensional gas-dynamic model [2].

1. GENERAL FORMULATION OF THE PROBLEM IN A MULTICOMPONENT MULTIVELOCITY APPROXIMATION

1.1. Description of the Experiment. The GOL-3 facility is a long solenoid with edge magnetic plugs. In the homogeneous part, the magnetic induction is $B = 4.5$ T, and the plug ratio is $H_{\max}/H_0 = 2$. The solenoid of length $L \approx 12$ m is filled with a homogeneous hydrogen (deuterium) plasma of diameter $D = 6$ cm and density

[1]Institute of Nuclear Physics, Siberian Division, Russian Academy of Sciences, Novosibirsk 630090. [2]Novosibirsk State University, Novosibirsk 630090. [3]Institute of Computational Technologies, Siberian Division, Russian Academy of Sciences, Novosibirsk 630090. Translated from Prikladnaya Mekhanika i Tekhnicheskaya Fizika, Vol. 42, No. 6, pp. 3–18, November–December, 2001. Original article submitted July 30, 2001.

0021-8944/01/4206-0929 $25.00

$n \approx 10^{15}$ cm^{-3}. The plasma column is heated by a powerful electron beam with an energy up to $eU_0 \approx 1$ MeV, a current up to $I_0 \approx 30$ kA, and a duration up to $\tau_b \approx 8$ μsec. The collective interaction of the beam with the plasma leads to heating of the plasma electrons to $T_e \approx 1$ keV with formation of a group of accelerated non-Maxwellian electrons with a density $n_h \approx 10^{13}$ cm^{-3} and a characteristic energy $\varepsilon_h \approx 10$ keV.

Before the beam switches on, a grain of a solid material (lithium deuteride, polyethylene, etc.) of mass 0.1–0.2 mg is injected into the center of the solenoid. After the beam switches on, the grain vaporizes, dissociates into atoms, and ionizes to form a dense plasma. As estimates show, the immediate heating of the grain by the electron beam is inappreciable because the mean free path of the beam electrons $l \approx 0.3$ cm is much larger than the grain size. The energy for heating the grain comes primarily from the thermal and superthermal electrons of the plasma and the delayed scattered electrons of the beam. Estimation of the dynamics of the processes shows that in $t \approx 0.5$ μsec, the grain vaporizes, the molecules dissociate, and the gas bunch is heated to $T \approx 0.1$–1.0 eV with expansion to approximately 1 mm at a rate of about $1.5 \cdot 10^5$ cm/sec. This state is taken as the initial one for simulation and numerical solution of the problem. As shown in experiments, the expansion and heating of the plasma cloud of the grain proceeds until this dense plasma is magnetized. Next, as in the model of two-step heating [3], the grain plasma absorbs the energy of the hot plasma and the high-velocity electrons accumulated in the 12-m solenoid. The energy content of the REB is sufficient that the energy accumulated in the grain plasma reached a value of about 1 keV/atom. The present simulation is carried out for a grain of lithium deuteride containing the isotope of lithium with a relative atomic weight of 6.

1.2. Collisional Characteristics and Magnetization of the Plasma. To determine the state of the plasma cloud, we estimated a number of its parameters. The results are given below.

1. At the stage of ionization of the gas–plasma mixture, the mixture components have identical temperatures (equilibration time $t \approx 10^{-10}$ sec). Since the dense gas–plasma bunch is characterized by a high collision frequency, the present calculations used an approximate model of ionization equilibrium. For $T_e \leqslant T_\alpha^*$, it is defined by the linear relation $f_\alpha(T_e) = \max\{0, (T_e - 1)/(T_\alpha^* - 1)\}$, where T_e and T_α^* are in electronvolts, and $f_\alpha \equiv 1$ at $T_e > T_\alpha^*$. For deuterium, the characteristic ionization temperature T^* is set equal to approximately 3 eV (as follows from the Saha formula), and for lithium, it is taken to be $T^* \approx 15$ eV, i.e., about 1/5–1/4 of the mean ionization energy of the atoms (13.6 eV for deuterium and approximately 70 eV for lithium). The electron density is given by

$$n_e = Z_{\rm D} n_{s\rm D} f_{\rm D}(T_e) + Z_{\rm Li} n_{s\rm Li} f_{\rm Li}(T_e), \tag{1}$$

where Z is the charging number ($Z_{\rm D} = 1$ and $Z_{\rm Li} = 3$) and n_s is the density of the atoms (charged and neutral); the subscripts D and Li correspond to deuterium and lithium, respectively.

2. The temperatures of the deuterium and lithium ions are nearly always equal (even at $r \approx 4$ cm, the equilibration time is $t < 10^{-6}$ sec).

3. The temperatures of the electrons and ions are nearly equal when the dimension of the bunch $r < 1.5$ cm [equilibration time $t < (0.1$–$0.3) \cdot 10^{-6}$ sec and further increases in proportion to $(rT^{1/2})^3$], and with expansion of the bunch, they can differ.

4. At the initial stage of expansion, the plasma is not magnetized. Magnetization of the plasma electrons is manifested at $r > r^* = 1.0$–1.5 cm. Hence, before this stage there is spherical expansion of the cloud, and then the transverse motion is determined by the rate of plasma diffusion across the magnetic field. Along the magnetic field there is free gas-dynamic expansion of the plasma, so that the expansion of the cloud is no longer spherical.

1.3. Combined Equations of Magnetohydrodynamics. Following studies [4, 5], we formulate a system of equations to describe the dynamics of a three-component plasma (ions of two sorts and electrons) in a magnetic field. Assuming that the velocities of the atoms are identical, we write the continuity equations for deuterium and lithium:

$$\frac{\partial n_{s\rm D}}{\partial t} + -er\,(n_{s\rm D}\boldsymbol{V}_i) = 0, \qquad \frac{\partial n_{s\rm Li}}{\partial t} + -er\,(n_{s\rm Li}\boldsymbol{V}_i) = 0. \tag{2}$$

According to the above ionization model, the densities of the ions are defined as $n_{\rm D} = n_{s\rm D} f_{\rm D}(T_e)$ and $n_{\rm Li} = n_{s\rm Li} f_{\rm Li}(T_e)$ and the electron density is determined from expression (1).

The equations of motion for the ions and electrons taking into account collisions have the form

$$(m_{\rm D} n_{\rm D} + m_{\rm Li} n_{\rm Li})\Big[\frac{\partial \boldsymbol{V}_i}{\partial t} + (\boldsymbol{V}_i \cdot \nabla)\boldsymbol{V}_i\Big]$$

$$= -\nabla[(n_{\rm D} + n_{\rm Li})kT_i] + e(Z_{\rm D} n_{\rm D} + Z_{\rm Li} n_{\rm Li})\Big[\boldsymbol{E} + (1/c)[\boldsymbol{V}_i \times \boldsymbol{H}]\Big] - \boldsymbol{R}_U - \boldsymbol{R}_T; \tag{3}$$

$$m_e n_e\Big[\frac{\partial \boldsymbol{V}_e}{\partial t} + (\boldsymbol{V}_e\cdot\nabla)\boldsymbol{V}_e\Big] = -\nabla(n_e kT_e) - en_e\Big[\boldsymbol{E} + (1/c)[\boldsymbol{V}_e\times\boldsymbol{H}]\Big] + \boldsymbol{R}_U + \boldsymbol{R}_T. \tag{4}$$

The expressions for the force of friction between the electrons and ions [4]

$$\boldsymbol{R}_U = \frac{m_e n_e}{\tau_e}\Big[0.44(\boldsymbol{V}_{i\parallel} - \boldsymbol{V}_{e\parallel}) + (\boldsymbol{V}_{i\perp} - \boldsymbol{V}_{e\perp})\Big(1 - \frac{5.52(\omega_e\tau_e)^2 + 0.56}{(\omega_e\tau_e)^4 + 10.8(\omega_e\tau_e)^2 + 1.05}\Big)\Big] = en_e(\ddot{\sigma}^{-1}\boldsymbol{j}) \tag{5}$$

and the formula for the thermal force

$$\boldsymbol{R}_T = n_e\Big(0.91\nabla_\parallel kT_e + \frac{4.45(\omega_e\tau_e)^2 + 0.95}{(\omega_e\tau_e)^4 + 10.8(\omega_e\tau_e)^2 + 1.05}\,\nabla_\perp kT_e$$

$$+ \frac{(\omega_e\tau_e)(1.5(\omega_e\tau_e)^2 + 1.78)}{(\omega_e\tau_e)^4 + 10.8(\omega_e\tau_e)^2 + 1.05}\,[\boldsymbol{h}\times\nabla kT_e]\Big) = n_e(\ddot{\chi}\nabla kT_e) \tag{6}$$

are obtained for the mean value of the ion charge $Z = 2$. Because in this approximation the ratios Z_α/m_α for ions of both sorts are equal, it follows that with identical initial velocities, their further velocities will also be equal, and this is used in the continuity equations (2). Here $\omega_e = eH/(m_e c)$ is the cyclotron electron frequency, $\tau_e = 3\sqrt{m_e}(kT_e)^{3/2}/(4\sqrt{2\pi}\lambda e^4 Z n_e)$ is the time of electron scattering by ions, λ is the Coulomb logarithm, k is the Boltzmann constant, $\boldsymbol{h}$ is a unit vector directed along the magnetic field, $\boldsymbol{j} = en_e(\boldsymbol{V}_i - \boldsymbol{V}_e) = (c/(4\pi))\,\mathrm{rot}\,\boldsymbol{H}$ is the current density in the plasma. In addition, expressions (5) and (6) contain the conductivity tensor $\ddot{\sigma}$ and the dimensionless thermal force tensor $\ddot{\chi}$.

At the initial stage, where the processes are determined by collisions, the expansion of the plasma bunch is spherically symmetric. Furthermore, the sliding of plasma layers is insignificant throughout the process. Therefore, the viscosity force in (3)–(6) is ignored.

Using Eqs. (3)–(6) and taking into account the equality of temperatures and velocities of the ions, we write the following equation of motion for the plasma (equation of one-fluid magnetohydrodynamics):

$$n_e M\,\frac{d\boldsymbol{V}}{dt} = -\nabla\Big[(n_{\mathrm{D}} + n_{\mathrm{Li}})kT_i + n_e kT_e\Big] + \frac{1}{c}\,[\boldsymbol{j}\times\boldsymbol{H}].$$

In this case, the last term of the equation can be brought to the form $-\nabla H^2/(8\pi) + (\boldsymbol{H}\cdot\nabla)\boldsymbol{H}/(4\pi)$ (see [5]). Here d/dt is the total derivative and M and $\boldsymbol{V}$ are the mean mass and velocity of a plasma particle:

$$M = \frac{m_{\mathrm{D}} n_{\mathrm{D}}}{n_e} + \frac{m_{\mathrm{Li}} n_{\mathrm{Li}}}{n_e} + m_e, \qquad \boldsymbol{V} = \frac{1}{M}\Big[\Big(\frac{m_{\mathrm{D}} n_{\mathrm{D}}}{n_e} + \frac{m_{\mathrm{Li}} n_{\mathrm{Li}}}{n_e}\Big)\boldsymbol{V}_i + m_e\boldsymbol{V}_e\Big].$$

Similarly to [5], we obtain the magnetic field equation. We divide Eq. (3) by $m_e n_e$ and (4) by $m_{\mathrm{D}} n_{\mathrm{D}} + m_{\mathrm{Li}} n_{\mathrm{Li}}$ and subtract from one the other, neglecting inertial terms and terms of order m_e/m_i. We obtain a relation between the electric field and the current density similar to Ohm's law. Next, performing the operation of rot and using Maxwell's equations

$$\mathrm{rot}\,\boldsymbol{E} = -\frac{1}{c}\Big(\frac{\partial \boldsymbol{H}}{\partial t}\Big) \tag{7}$$

and $\mathrm{rot}\,\boldsymbol{H} = 4\pi\boldsymbol{j}/c$, we obtain the required equation

$$\frac{\partial \boldsymbol{H}}{\partial t} = \mathrm{rot}\,[\boldsymbol{V}\times\boldsymbol{H}] - \frac{c}{4\pi e}\,\mathrm{rot}\,\frac{[\mathrm{rot}\,\boldsymbol{H}\times\boldsymbol{H}]}{n_e}$$

$$- \frac{c}{en_e}\,[\nabla n_e\times\nabla kT_e] + \frac{c^2}{4\pi}\,\ddot{\sigma}^{-1}\,\Delta\boldsymbol{H} + \frac{c^2}{4\pi e n_e}\,\mathrm{rot}\,(\ddot{\chi}\nabla kT_e). \tag{8}$$

The energy-balance equation is written with allowance for the heating of the cloud by the electron beam and by the superthermal electrons of the background plasma, energy expenditures in ionization of the cloud and transfer of the thermal energy to the ions of the cloud [2]:

$$\begin{gathered}\frac{3}{2}\,\frac{\partial(n_s kT_i)}{\partial t} + \frac{3}{2}\,\mathrm{div}\,(n_s kT_i\boldsymbol{V}_i) + n_s kT_i\,\mathrm{div}\,\boldsymbol{V}_i = \mathrm{div}\,(\ddot{\varkappa}_i\nabla kT_i) + Q_i,\\ \frac{3}{2}\,\frac{\partial(n_e kT_e)}{\partial t} + \frac{3}{2}\,\mathrm{div}\,(n_e kT_e\boldsymbol{V}_e) + n_e kT_e\,\mathrm{div}\,\boldsymbol{V}_e = \mathrm{div}\,(\ddot{\varkappa}_e\nabla kT_e) + Q_e.\end{gathered} \tag{9}$$

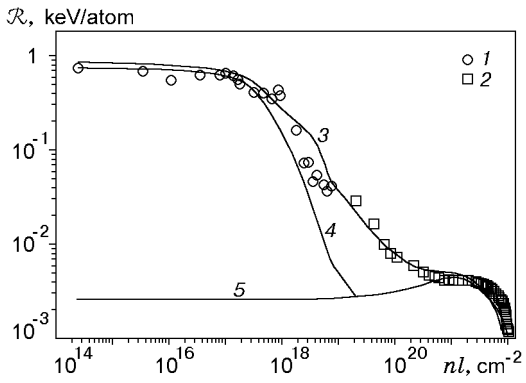

Fig. 1. Results of experiments on absorption of electrons by a hydrogen cloud and a graphite target: points 1 and 2 show the distributions of the energy absorbed by the hydrogen cloud and the graphite target, respectively; curves 3, 4, and 5 are the energy contribution from superthermal electrons, thermal (Maxwellian) electrons, and beam electrons, respectively.

Here the source of heating of the bunch electrons

$$Q_e = \frac{\partial E}{\partial t} - \frac{\partial(\varepsilon_i^{\mathrm{D}} + \varepsilon_i^{\mathrm{Li}})}{\partial t} + \frac{1}{2}\,\frac{n_e}{\tau_e}\,\frac{m_e}{M}\,k(T_i - T_e)$$

contains the above-mentioned components, and

$$\varepsilon_i^{\mathrm{D}} \approx n_{\mathrm{D}}\Big[30 - 16.4\exp\Big(-\frac{5\cdot 10^{13}}{n}\Big)\Big]\,\frac{5.45}{T\exp\left((n/(1.37\cdot 10^{14}))^{0.26}\right)} \tag{10}$$

is the price of ionization of deuterium atoms, $\varepsilon_i^{\mathrm{Li}} \approx 70$ eV is the price of ionization of lithium atoms, i.e., the energy absorbed by the atoms of the cloud that is expended in excitation and ionization during their heating, and $\partial E/\partial t$ is the heating of the cloud due to deceleration in it of superthermal plasma electrons and beam electrons with an energy of 5–1000 keV, which interact with the plasma. In (10), $\varepsilon_i^{\mathrm{D}}$ and T are in eV and n_{D} is in cm^{-3}. The heating of the cloud is described by the expression

$$\frac{\partial E(nl,t)}{\partial t} = \frac{P(t)\eta_h}{S}\int\limits_{\varepsilon_{\min}}^{\infty} f(nl,\varepsilon)\,\frac{\varphi(\varepsilon)\,d\varepsilon}{\varepsilon},$$

where $P(t)$ is the REB power transferred to superthermal electrons with efficiency η_h, S is the section of the beam, $\varphi(\varepsilon)$ is the spectrum of energy of superthermal electrons, $f(nl,\varepsilon)$ is the function of absorption of electrons with energy ε at the length corresponding to the linear density $nl = \int n\,dl$, which given with the normalization $\int f(nl,\varepsilon)\,d(nl) = \varepsilon$. In the physical model considered, the heating of the cloud is described by an experimental heat-release distribution over the depth of the target $\mathcal{R}(nl)$ per a pulse of the REB (Fig. 1). This makes it possible to immediately take into account the real energy distribution of the electrons of the background plasma and the beam:

$$\frac{\partial E}{\partial t} = \frac{P(t)}{\int P(t)\,dt}\,\mathcal{R}(nl). \tag{11}$$

Here $P(t)$ is the power of the beam and nl is reckoned from the boundary of the calculation domain.

The term $Q_i = (1/2)(n_e/\tau_e)(m_e/M)k(T_e - T_i)$ describes the heating of ions due to electron–ion collisions.

The electron heat conductivities in the cloud for $Z = 2$ are specified as follows [4]:

— for longitudinal conductivity,

$$æ_{e\|} = 4.9\,\frac{n_e k T_e \tau_e}{m_e};$$

— for transverse conductivity,

$$æ_{e\perp} = \frac{n_e k T_e \tau_e}{m_e} \frac{4(\omega_e\tau_e)^2 + 5.1}{(\omega_e\tau_e)^4 + 10.8(\omega_e\tau_e)^2 + 1.05};$$

— for "oblique" conductivity,

$$æ_{e\wedge} = \frac{n_e k T_e \tau_e}{m_e} \frac{(\omega_e\tau_e)(2.5(\omega_e\tau_e)^2 + 15.4)}{(\omega_e\tau_e)^4 + 10.8(\omega_e\tau_e)^2 + 1.05};$$

so that the heat flux is equal to $\boldsymbol{q}_T^e = -æ_{e\|}\nabla_\| kT_e - æ_{e\perp}\nabla_\perp kT_e - æ_{e\wedge}[\boldsymbol{h}\times\nabla kT_e]$. It should be noted that in the collective interaction of the beam with the plasma, experiments and calculations [2] revealed suppression of the electron heat conductivity by a factor of $\zeta_{\max} \approx 10^2$–$10^3$, which was explained by an increase in the effective frequency of electron collisions for developed Langmuir turbulence. The local turbulence level depends on the power of the beam and the plasma density because of the stabilizing effect of electron collisions on the development of beam instability [2]. Furthermore, for a plasma density above a certain critical value of $n_c \approx 3\cdot 10^{15}$ cm^{-3}, collective interaction of the beam with the plasma is practically absent. These effects are allowed for in the model phenomenologically, by a numerical coefficient that depends on the beam power P and the electron density n_e: $ëë_e^* = ëë_e/(1+\zeta_{\max}\sqrt{P(t)/P_{\max}}\,\max\{0,\log(n_c/n_e)\})$.

Similarly, the ion heat conductivity is defined as

$$æ_{i\|} = 3.9\,\frac{n_s k T_i \tau_i}{m_i}, \qquad æ_{i\perp} = 2\,\frac{n_s k T_i \tau_i}{m_i}\,\frac{2(\omega_i\tau_i)^2 + 2.6}{(\omega_i\tau_i)^4 + 2.7(\omega_i\tau_i)^2 + 0.677},$$

$$æ_{i\wedge} = 2\,\frac{n_s k T_i \tau_i}{m_i}\,\frac{(\omega_i\tau_i)(2.5(\omega_i\tau_i)^2 + 4.65)}{(\omega_i\tau_i)^4 + 2.7(\omega_i\tau_i)^2 + 0.677}.$$

Suppression of the ion heat conductivity is ignored in the model because it was not revealed in experiments.

1.4. Initial Conditions. The initial conditions of the problem are determined by the state of the system in an experiment 0.5 μsec after the beam switches on. The density and temperature of the background plasma are $n \approx 10^{15}$ cm^{-3} and $T_e \approx 10$ eV, respectively, and the velocity is $\boldsymbol{V} = 0$. The parameters of the plasma cloud are as follows: $n_s \approx 0.5\cdot 10^{21}$ cm^{-3}, $r_0 \approx 1$ mm, $T_0 \approx 1$ eV, and $V_0(r) \approx 1.5\cdot 10^5 (r/r_0)$ cm/sec. By this moment, the power of the beam reaches $P \approx 10$ GW (maximum power $P_{\max} \approx 30$ GW at the moment $t_{\max} \approx 3$ μsec) for a beam duration of 6 μsec and a total energy content of about 150 kJ (data of a typical experiment).

1.5. Boundary Conditions. On the axis of the system, the boundary conditions have the standard form: $\partial/\partial r = 0$; on the boundaries of the simulation domain along the z coordinate, $\partial(T_e, T_i, n_e, n_i, \boldsymbol{V}_e, \boldsymbol{V}_i, \boldsymbol{H})/\partial z = 0$. In the domain considered, the electron temperature is determined from the energy contribution from superthermal and beam electrons by dependences (11) using Fig. 1 and Eqs. (9). On the outer boundary of the plasma located close to the metal surface of the vacuum tube of the facility, the boundary conditions for the plasma depend on how close the boundary is to the tube. The magnetic field inside the tube should satisfy the condition of conservation of the field flux in the tube $\Phi = \int_0^R 2\pi r H(r)\,dr$.

The solution of the complete problem involves simultaneous solution of the Eqs. (2)–(4) and (7)–(9) subject to the initial and boundary conditions.

2. ONE-FLUID MODEL

2.1. Formulation of the Problem. We consider the propagation of a dense plasma cloud heated by an extraneous source in an external magnetic field. At the initial moment, the plasma cloud is assumed to be axisymmetric with a density several orders of magnitude higher than the density of the background plasma surrounding the cloud. Under the action of hydrodynamic and magnetic pressures and the external heat source, the plasma cloud begins to expand in the background plasma. The flow is considered axisymmetric and is simulated as the propagation of the plasma cloud in a certain cylindrical volume filled with a low-density plasma and located in a longitudinal magnetic field. In a magnetohydrodynamic approximation, the basic equations for plasma heating and propagation can be written in vector form

$$\frac{\partial n_s}{\partial t} + \text{–}er\,(n_s \boldsymbol{V}) = 0,$$

$$n_s M\Big(\frac{\partial \boldsymbol{V}}{\partial t} + (\boldsymbol{V}\cdot\nabla)\boldsymbol{V}\Big) = \frac{1}{c}\,[\boldsymbol{j}\times\boldsymbol{H}] - \nabla(n_s T), \tag{12}$$

$$\frac{3}{2}\,\frac{\partial(n_s T)}{\partial t} + \frac{3}{2}\,\text{–}er\,(n_s T\boldsymbol{V}) + (n_s T)\text{–}er\boldsymbol{V} = \text{–}er\,(k_e\nabla T) + Q;$$

$$\frac{\partial \boldsymbol{H}}{\partial t} = \operatorname{rot}[\boldsymbol{V}\times\boldsymbol{H}] + \frac{c}{en_s}[\nabla n_s\times\nabla T] + \frac{c^2}{4\pi\sigma}\,\Delta\boldsymbol{H}. \tag{13}$$

Here n_s is the plasma density, M is the mass of a particle, $\boldsymbol{V}$ is the velocity, c is speed of light, $\boldsymbol{H}$ is the magnetic field, $\boldsymbol{j} = (c/(4\pi))\operatorname{rot}\boldsymbol{H}$ is the current density, T is the temperature of the plasma, σ is the longitudinal conductivity of the plasma, k_e is the electron heat conductivity, e is the electron charge, Q is the external heat source which simulates plasma heating by a relativistic electron beam.

The external magnetic field is directed along the z axis. By virtue of flow symmetry, the problem does not depend on the angular coordinate φ but contains all components of the velocity and magnetic field along the z, r, and φ directions of cylindrical coordinates. For closure of system (12), (13), the equation of state is specified as $p = n_s T$, the heat conductivity is considered constant as well as the longitudinal conductivity σ.

The calculation domain is chosen as a section of a cylinder of length L and radius R with a dense plasma cloud located at its center. By virtue of the symmetry of the problem, on the axis $r = 0$, the following conditions were imposed

$$\frac{\partial n_s}{\partial r} = \frac{\partial v_z}{\partial r} = \frac{\partial p}{\partial r} = \frac{\partial H_z}{\partial r} = v_r = v_\varphi = H_r = H_\varphi = 0.$$

The upper and lateral boundaries of the cylinder were specified far enough from the center, and it was assumed that the perturbations from the cloud do not reach the boundaries because of the effect of magnetohydrodynamic forces. On the boundaries, the conditions for the background plasma were specified as follows: $H_r = H_\varphi = v_r = v_z = v_\varphi = 0$, $p = p_\infty$, $n_s = n_{s\infty}$, and $H_z = H_{z\infty}$.

During the solution, we varied the initial density of the cloud, the external magnetic field, and the power of the heat source Q. The solution of the present problem was unsteady and was sought in the region $L\times R$ at various times. In the absence of a magnetic field and a heat source, the solution was sought before the time when the perturbations from the plasma cloud reached the boundaries of the region, and in their presence, the solution was sought before formation of the main structure of the flow.

To construct of a numerical algorithm, it is convenient to write the basic equations (12) and (13) in vector form as two systems of equations:

$$\frac{\partial \boldsymbol{U}}{\partial t} = -(\boldsymbol{W}_r^0 + \boldsymbol{W}_z^0) + \boldsymbol{R}^0 = -\boldsymbol{W}^0; \tag{14}$$

$$\frac{\partial \boldsymbol{f}_1}{\partial t} = -(\boldsymbol{W}_r^1 + \boldsymbol{W}_z^1) + \boldsymbol{R}^1 = -\boldsymbol{W}^1. \tag{15}$$

System (14) describe hydrodynamic processes, and (15) are the magnetic-field equations. Here

$$\boldsymbol{U} = \begin{pmatrix} n_s \\ n_s v_r \\ n_s v_\varphi \\ n_s v_z \\ p \end{pmatrix}, \qquad \boldsymbol{W}_r^0 = \begin{pmatrix} \dfrac{1}{r}\,\dfrac{\partial(r n_s v_r)}{\partial r} \\ \dfrac{1}{r}\,\dfrac{\partial(r n_s v_r^2)}{\partial r} + \dfrac{1}{M}\,\dfrac{\partial p}{\partial r} - \dfrac{n_s v_\varphi^2}{r} \\ \dfrac{1}{r}\,\dfrac{\partial(r n_s v_r v_\varphi)}{\partial r} + \dfrac{n_s v_r v_\varphi}{r} \\ \dfrac{1}{r}\,\dfrac{\partial(r n_s v_r v_z)}{\partial r} \\ \dfrac{1}{r}\Big(\dfrac{\partial(r p v_r)}{\partial r} + \dfrac{2}{3}\,p\,\dfrac{\partial(r v_r)}{\partial r}\Big) - \dfrac{2}{3}\,\dfrac{1}{r}\,\dfrac{\partial}{\partial r}\Big(r k_e\,\dfrac{\partial T}{\partial r}\Big) \end{pmatrix},$$

$$\boldsymbol{W}_z^0 = \begin{pmatrix} \dfrac{\partial(n_s v_z)}{\partial z} \\ \dfrac{\partial(n_s v_z v_r)}{\partial z} \\ \dfrac{\partial(n_s v_z v_\varphi)}{\partial z} \\ \dfrac{\partial(n_s v_z^2)}{\partial z} + \dfrac{1}{M}\dfrac{\partial p}{\partial z} \\ \dfrac{\partial(p v_z)}{\partial z} + \dfrac{2}{3}p\dfrac{\partial v_z}{\partial z} - \dfrac{2}{3}\dfrac{\partial}{\partial z}\Big(k_e\dfrac{\partial T}{\partial z}\Big) \end{pmatrix},$$

$$\boldsymbol{R}^0 = \begin{pmatrix} 0 \\ \dfrac{1}{4\pi M}\Big(H_z\dfrac{\partial H_r}{\partial z} - H_z\dfrac{\partial H_z}{\partial r} - \dfrac{H_\varphi}{r}\dfrac{\partial(rH_\varphi)}{\partial r}\Big) \\ \dfrac{1}{4\pi M}\Big(\dfrac{H_r}{r}\dfrac{\partial(rH_\varphi)}{\partial r} + H_z\dfrac{\partial H_\varphi}{\partial z}\Big) \\ \dfrac{1}{4\pi M}\Big(-H_\varphi\dfrac{\partial H_\varphi}{\partial z} - H_r\dfrac{\partial H_r}{\partial z} + H_r\dfrac{\partial H_z}{\partial r}\Big) \\ 2Q/3 \end{pmatrix},$$

$$\boldsymbol{f}_1 = \begin{pmatrix} H_r \\ H_\varphi \\ H_z \end{pmatrix}, \qquad \boldsymbol{W}_r^1 = \begin{pmatrix} -\dfrac{c^2}{4\pi\sigma}\dfrac{1}{r}\dfrac{\partial}{\partial r}\Big(r\dfrac{\partial H_r}{\partial r}\Big) \\ \dfrac{\partial}{\partial r}(v_r H_\varphi - v_\varphi H_r) - \dfrac{c^2}{4\pi\sigma}\dfrac{1}{r}\dfrac{\partial}{\partial r}\Big(r\dfrac{\partial H_\varphi}{\partial r}\Big) \\ -\dfrac{1}{r}\dfrac{\partial}{\partial r}(rv_z H_r - rv_r H_z) - \dfrac{c^2}{4\pi\sigma}\dfrac{1}{r}\dfrac{\partial}{\partial r}\Big(r\dfrac{\partial H_z}{\partial r}\Big) \end{pmatrix},$$

$$\boldsymbol{W}_z^1 = \begin{pmatrix} \dfrac{\partial}{\partial z}(v_z H_r - v_r H_z) - \dfrac{c^2}{4\pi\sigma}\dfrac{\partial}{\partial z}\Big(\dfrac{\partial H_r}{\partial z}\Big) \\ -\dfrac{\partial}{\partial z}(v_\varphi H_z - v_z H_\varphi) - \dfrac{c^2}{4\pi\sigma}\dfrac{\partial}{\partial z}\Big(\dfrac{\partial H_\varphi}{\partial z}\Big) \\ -\dfrac{c^2}{4\pi\sigma}\Big(\dfrac{\partial H_z}{\partial z}\Big) \end{pmatrix},$$

$$\boldsymbol{R}^1 = \begin{pmatrix} 0 \\ \dfrac{c}{en_s}\dfrac{1}{r}\Big(\dfrac{\partial T}{\partial r}\dfrac{\partial n_s}{\partial z} - \dfrac{\partial T}{\partial z}\dfrac{\partial n_s}{\partial r}\Big) \\ 0 \end{pmatrix}.$$

We note that the equations of continuity, motion, and magnetic induction are written in divergent form, and the energy equation is written in nondivergent form.

Along with Eqs. (14) and (15), we consider the following operator-vector equations in nondivergent form:

$$\frac{\partial \boldsymbol{f}}{\partial t} = -(\Omega_1^0 + \Omega_2^0)\boldsymbol{f} + \boldsymbol{S} = -(A^{-1})\boldsymbol{W}^0; \tag{16}$$

$$\frac{\partial \boldsymbol{f}_1}{\partial t} = -(\Omega_1^1 + \Omega_2^1)\boldsymbol{f}_1 + \boldsymbol{R}^1 = -\boldsymbol{W}^1. \tag{17}$$

Here $A = \partial \boldsymbol{U}/\partial \boldsymbol{f}$, $\boldsymbol{f} = (n_s, v_r, v_\varphi, v_z, p)^{\mathrm{t}}$, $\Omega_1^0\boldsymbol{f} = A^{-1}\boldsymbol{W}_z^0$, $\Omega_2^0\boldsymbol{f} = A^{-1}\boldsymbol{W}_z^0$, $\boldsymbol{S} = \boldsymbol{R}/M$, $\Omega_1^1\boldsymbol{f}_1 = \boldsymbol{W}_r^1$, and $\Omega_2^1\boldsymbol{f}_1 = \boldsymbol{W}_z^1$.

2.2. Numerical Algorithm. In the calculation domain $L \times R$, we introduce a difference grid with constant steps in space $h_r = R/I$, $h_z = L/J$, where I and J are the numbers of grid sizes along the r and z directions, respectively. The differential operators $\partial/\partial r$ and $\partial/\partial z$ are approximated by the difference operators Λ_1^k and Λ_2^k

of order k, where $k = 1, 2, \ldots$ (the superscript k is omitted below). The convective terms $v_r\partial/\partial r$ and $v_z\partial/\partial z$ in Eqs. (16) and (17) are approximated by one-sided difference operators of the first order ($k = 1$) with allowance for the sign of the velocities v_r and v_z. The terms with pressure (magnetic and gas-dynamic) are approximated by the formulas conjugate to the convective terms (see [6]), and the second derivatives are approximated by symmetric three-point difference operators of the second order. For example, the approximation formulas in the r direction are

$$v_r\frac{\partial}{\partial r} \approx v_r\Lambda_1, \qquad v_r\Lambda_1 = \begin{cases} v_r\Lambda_{1-}, & v_r \geqslant 0, \\ v_r\Lambda_{1+}, & v_r < 0, \end{cases}$$
$$\Lambda_{1-}f_l = \frac{f_l - f_{l-1}}{h_r}, \qquad \Lambda_{1+}f_l = \frac{f_{l+1} - f_l}{h_r}, \qquad \bar{\Lambda}_1 = \begin{cases} \Lambda_{1+}, & v_r \geqslant 0, \\ \Lambda_{1-}, & v_r < 0, \end{cases} \tag{18}$$
$$\Lambda_1 a\Lambda_1 f_l = [a_{l+1/2}(f_{l+1} - f_l) - a_{l-1/2}(f_l - f_{l-1})]/h_r^2, \quad a_{l\pm1/2} = (a_l + a_{l\pm1})/2.$$

Similarly, the vector operators $\boldsymbol{W}_r^s$, $\boldsymbol{W}_z^s$, and $\boldsymbol{R}^s$ ($s = 0, 1$) in Eqs. (14) and (15) are approximated deferentially with the first or second orders.

With allowance for the notation (18), the difference matrix operators Ω_1^0 and Ω_2^0 are written as

$$\Omega_1^0 = \begin{pmatrix} (1/r)\Lambda_1 r v_r & 0 & 0 & 0 & 0 \\ 0 & v_r\Lambda_1 & -v_\varphi/r & 0 & (1/(Mn_s))\bar{\Lambda}_1 \\ 0 & v_\varphi/r & v_r\Lambda_1 + v_r/r & 0 & 0 \\ 0 & 0 & 0 & v_r\Lambda_1 & 0 \\ 0 & (5/3)(p/r)\Lambda_1 & 0 & 0 & v_r\Lambda_1 - (2/3)\Lambda_1 r k_e \Lambda_1 (1/n_s) \end{pmatrix},$$

$$\Omega_2^0 = \begin{pmatrix} \Lambda_2 v_z & 0 & 0 & 0 & 0 \\ 0 & v_z\Lambda_2 & 0 & 0 & 0 \\ 0 & 0 & v_z\Lambda_2 & 0 & 0 \\ 0 & 0 & 0 & v_z\Lambda_2 & (1/(Mn_s))\bar{\Lambda}_2 \\ 0 & 0 & 0 & (5/3)p\Lambda_2 & v_z\Lambda_2 - (2/3)\Lambda_2 k_e \Lambda_2 (1/n_s) \end{pmatrix}.$$

The matrix operators Ω_1^1 and Ω_2^1, which approximate the equations of magnetic induction in divergent form can be written similarly.

To construct an economical difference scheme, we perform splitting of the operators Ω_j^0 into physical processes, i.e., we write them as

$$\Omega_1^0 = \Omega_{11}^0 + \Omega_{12}^0,$$

where

$$\Omega_{11}^0 = \begin{pmatrix} 0 & 0 & 0 & 0 & 0 \\ 0 & 0 & -v_\varphi/r & 0 & (1/(Mn_s))\bar{\Lambda}_1 \\ 0 & v_\varphi/r & v_r/r & 0 & 0 \\ 0 & 0 & 0 & 0 & 0 \\ 0 & (5/3)(p/r)\Lambda_1 & 0 & 0 & v_r\Lambda_1 - (2/(3r))\Lambda_1 r k_e \Lambda_1 (1/n_s) \end{pmatrix}.$$

The operator Ω_{11}^0 contains terms with pressure, the free terms from the equations of motion, and all terms of the energy equation along the r direction, and the operator

$$\Omega_{12}^0 = \begin{pmatrix} (1/r)\Lambda_1 r v_r & 0 & 0 & 0 & 0 \\ 0 & v_r\Lambda_1 & 0 & 0 & 0 \\ 0 & 0 & v_r\Lambda_1 & 0 & 0 \\ 0 & 0 & 0 & v_r\Lambda_1 & 0 \\ 0 & 0 & 0 & 0 & 0 \end{pmatrix}$$

contains convective terms from the equations of motion and all terms of the continuity equation. We note that the continuity equation is approximated in divergent form. Splitting into physical processes along the z direction is introduced similarly, i.e., the operator Ω_2^0 is written as $\Omega_2^0 = \Omega_{21}^0 + \Omega_{22}^0$.

For numerical solution of the equations of gas dynamics (14) or (16), we consider the following scheme of approximate factorization with splitting of the operators into physical processes and spatial directions [7]:

$$\prod_{j=1}^{2}(I + \tau\alpha\Omega_{j1}^0)(I + \tau\alpha\Omega_{j2}^0)\frac{f^{n+1} - f^n}{\tau} = -(A^{-1})^n(W^0)^n \tag{19}$$

or the equivalent fractional-step scheme

$$\begin{gathered}\xi^n = -(A^{-1})^n(W^0)^n, \qquad (I + \tau\alpha\Omega_{11}^0)\xi^{n+1/4} = \xi^n, \qquad (I + \tau\alpha\Omega_{12}^0)\xi^{n+2/4} = \xi^{n+1/4},\\ (I + \tau\alpha\Omega_{21}^0)\xi^{n+3/4} = \xi^{n+2/4}, \qquad (I + \tau\alpha\Omega_{22}^0)\xi^{n+1} = \xi^{n+3/4}, \qquad f^{n+1} = f^n + \tau\xi^{n+1},\end{gathered} \tag{20}$$

where τ is a time step, n is the time-step number, and $0 \leqslant \alpha \leqslant 1$ is the weight parameter. The difference scheme (19) or (20) approximates the basic equations (12) with order $O(\tau + h)$. Furthermore, as follows from the form of the operators Ω_{jl}^0, the fractional-step scheme is implemented by scalar three-point runs, similar to the splitting scheme [7]. The equations on the right side of the scheme are approximated in conservative form, which improves the calculation accuracy. We note that along with gas-dynamic terms, the vector $(A^{-1})^n(W^0)^n$ contains terms with magnetic pressure and is approximated in the nth known layer. Thus, in the difference scheme (19), the magnetohydrodynamic terms are approximated explicitly. In the absence of a magnetic field, the difference scheme (19) is unconditionally stable (in a linear approximation). This makes it possible to vary the grid steps (time and spatial) to obtain a numerical solution with the required accuracy. With a nonzero magnetic field, the unconditional stability of the scheme is disturbed, but, as calculations show, the step τ can be chosen over a wide range of values. After finding gas-dynamic parameters in the new $(n + 1)$th time layer, the magnetic-induction equations (15) are solved. To solve them numerically, we constructed the following scheme of approximate factorization with operator splitting into spatial directions:

$$(I + \tau\alpha\Omega_1^1)(I + \tau\alpha\Omega_2^1)\frac{f_1^{n+1} - f_1^n}{\tau} = -(W^1)^n \tag{21}$$

or the equivalent fractional-step scheme

$$\begin{gathered}\xi_1^n = -(W^1)^n, \qquad (I + \tau\alpha\Omega_1^1)\xi_1^{n+1/2} = \xi_1^n,\\ (I + \tau\alpha\Omega_2^1)\xi_1^{n+1} = \xi_1^{n+1/2}, \qquad f_1^{n+1} = f_1^n + \tau f_1^{n+1}.\end{gathered} \tag{22}$$

As follows from the form of the operators Ω_j^1, the difference fractional-step scheme (22) is implemented by scalar runs and is unconditionally stable for $\alpha \geqslant 0.5$.

The explicit representation for the magnetic field in scheme (19) leads to disturbance of the unconditional stability of schemes (19) and (21) but allows one to effectively obtain a solution of the equations by scalar runs, which makes this algorithm economical. Moreover, this computational algorithm can also be employed for more complex models.

2.3. Calculation Results. The difference scheme proposed above was tested by solving simplified problems in order to assess the calculation accuracy and stability of the algorithm. The calculations confirmed theoretical estimates of the stability of the scheme. This allows grid parameters to be varied over a wide range to obtain a solution in minimum computing time. A solution of adequate accuracy (of the order of the accuracy of the physicomathematical model) can be obtained on 300×150 calculation grids. Further double increase in the number of nodes in each direction practically did not lead to a change of the solution, and the calculation error was not more than 5%. The largest difference was observed for the symmetry axis, which is explained by the choice of a cylindrical coordinate system, which has a mathematical singularity at $r = 0$.

In the first series of calculations, we studied the propagation of a gas cloud located at the center of the calculation domain in the absence of a magnetic field. At the initial time, unperturbed values were specified in the domain (below, all quantities are given in dimensionless units); the number density and pressure are obtained by normalization by the corresponding values of the background plasma, and the characteristic time and distance are 1 μsec and 1 cm, respectively): $n_{s\infty} = 1.0$, $p_\infty = 1.0$, $v_{r\infty} = v_{z\infty} = 0$, and $H_{r\infty} = H_{\varphi\infty} = H_{z\infty} = 0$, and in the gas cloud, the density and pressures were varied from the background values to n_{sc} and $p_c \equiv 10^2$–10^3, respectively

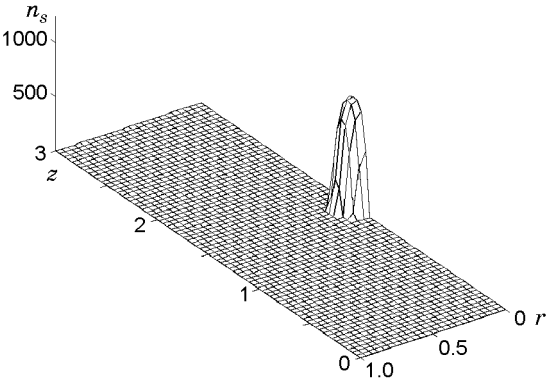

Fig. 2. Initial configuration of the density field.

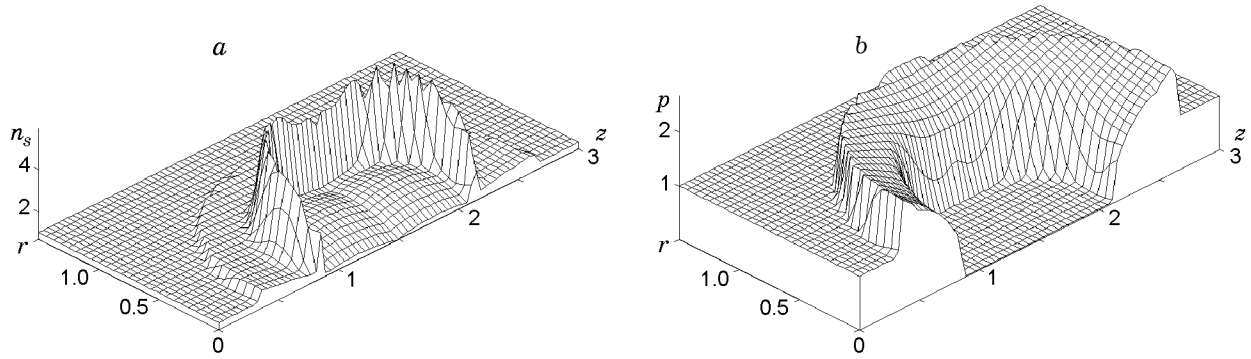

Fig. 3. Expansion in the absence of a magnetic field: (a) density distribution; (b) pressure distribution.

(Fig. 2). Due to the initial pressure gradient, the cloud began to expand. We note that for the explicit scheme, occurrence of such flow regimes with a pressure gradient and a density of about 10^3 seems almost impossible because it requires a very small step in time. The problem had two types of symmetry — axial symmetry about the axis of the calculation domain at $r = 0$ and mirror symmetry about the plane passing through the center of the gas cloud perpendicular to the z axis.

Figure 3 gives a typical flow pattern for the time $t = 0.5$ with a pressure drop and density at the initial moment $p_c/p_\infty = n_{sc}/n_{s\infty} = 10^3$. The result obtained adequately describes the spherically symmetric propagation of the cloud. We note that the observed irregularities in the region of maximum density are due to inaccuracies of algorithms during visualization. Two density waves are formed in regions of maximum pressure gradients. At the same time, a region of lower density is formed inside the cloud. Its density is comparable to the density of the background plasma and its temperature is several orders of magnitude lower than the initial value. The plasma temperature reduces in the region between the wave fronts. We note that in these calculations, the heat conductivity was set equal to zero. The dimensionless phase velocity of the front is $V_{\rm ph} = 2.07$ for the external wave and 1.29 for the internal wave. The speed of sound C_s in the initial state is also 1.29. Thus, in the system under the given initial conditions, a shock wave with a Mach number $V_{\rm ph}/C_s \approx 1.6$ is formed.

For comparison, Fig. 4 gives the density distribution at the same time for the same initial conditions for the one-dimensional problem corresponding to expansion of a plasma cylinder of infinite extent (and not a sphere, as in Fig. 3). Unlike in the spherical case, here the residual density at the center of the cloud remains well beyond the background value.

In further calculations, we studied the effect of a magnetic field on the propagation of the plasma cloud. This effect was characterized by the coefficient Φ (equal to the double ratio of magnetic-field pressure to gas-kinetic pressure under the given initial conditions), which was varied over a wide range ($0 \leqslant \Phi < 10^2$). Because the magnetic field is directed along the z axis, the resulting magnetohydrodynamic forces act across the z axis in the direction of the radius. They confine the lateral expansion of the magnetized plasma cloud, which can penetrate through the magnetic field by collisional diffusion, which depends on electron conduction. Figure 5 shows pressure

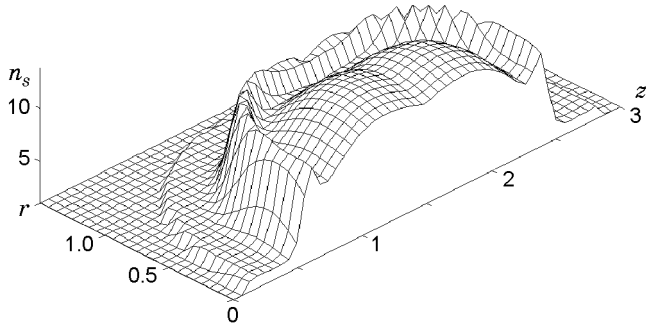

Fig. 4. Calculation results for the one-dimensional problem.

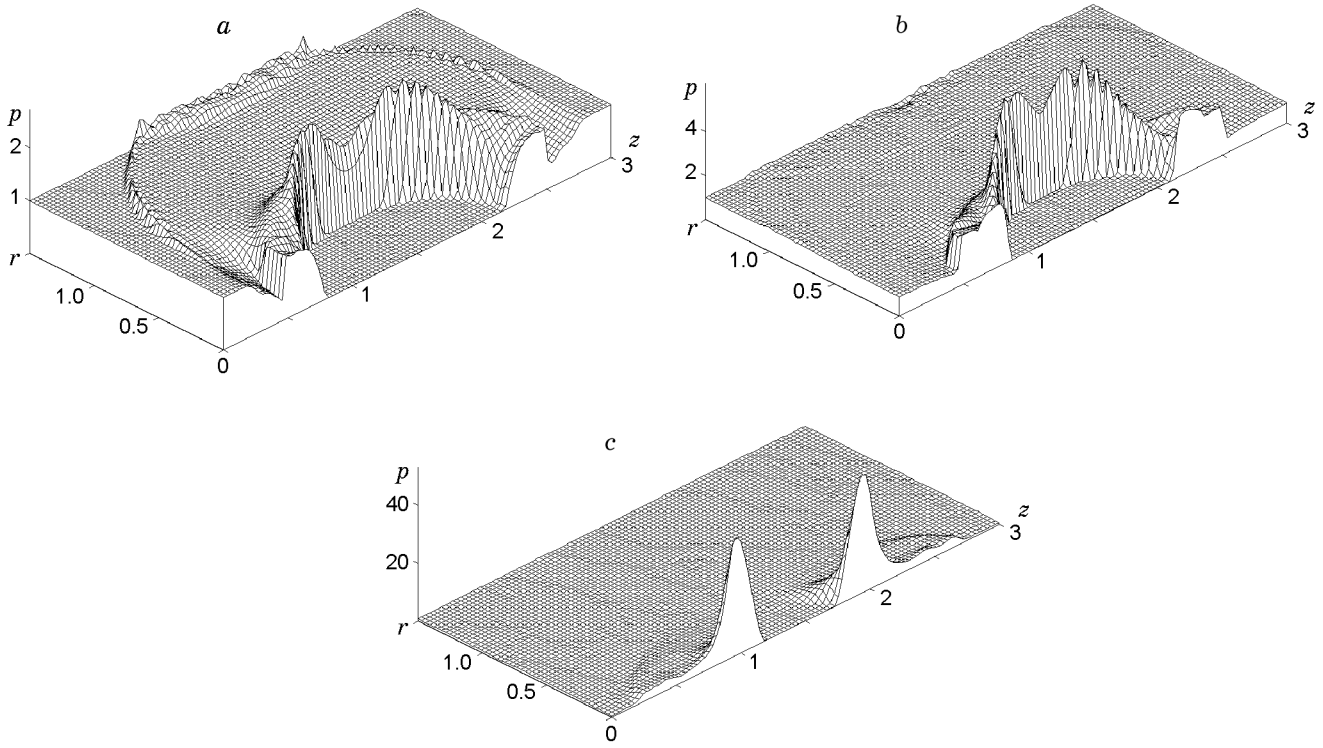

Fig. 5. Expansion in a magnetic field for $\Phi = 5$ (a), 15 (b), and 30 (c).

profiles at the time $t = 0.5$ for values $\Phi = 5$, 15, and 30. Amplification of the magnetic field (increase of Φ) leads to an increase in shock-wave velocity in the radial direction. This is explained by an increase in the elasticity of the plasma due to magnetic field freezing-in [8]. In this case, the pressure and density amplitudes at the shock-wave front decrease by one or two orders of magnitude. Most of the plasma confined by the magnetic field remains in the region of the internal front, whose transverse velocity decreases with increase in magnetic field (Fig. 5a and b). Finally, in the case of $\Phi = 30$ (Fig. 5c), the transverse expansion of the cloud practically ceases, and it is divided into two parts, which spread along the axis.

Figure 6 gives the mean radius of the cloud δ versus the magnitude of the magnetic field at $t = 0.5$ (the mean radius of the cloud was determined by the region in which half maximum density of the cloud was reached). An increase of the parameter Φ leads to a decrease in the expansion region, and for large values of Φ, the plasma spreads primarily in the z direction.

Figure 7 shows the change of the mean radius of the cloud δ with time for fixed magnitudes of the magnetic field ($\Phi = 0$, 10, 15, and 30). As follows from Fig. 7, the occurrence of a magnetic field limits the transverse expansion of the cloud, and its maximum radius decreases with increase of the coefficient Φ.

In the experiment of [1], the expansion of the cloud was photographed in the ultraviolet spectrum. The transverse dimensions of the cloud determined from the photographs at the times $t = 2$, 4, and 6 μsec are 0.5–1.0,

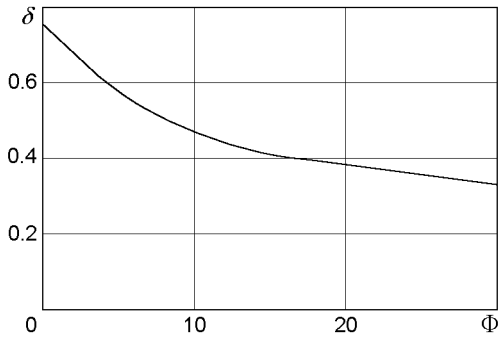

Fig. 6

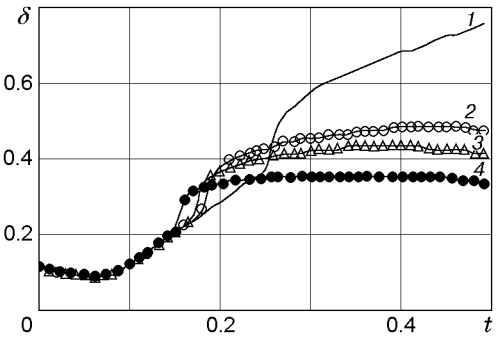

Fig. 7

Fig. 6. Mean radius of the cloud δ versus Φ at $t = 0.5$.

Fig. 7. Mean radius δ versus time for $\Phi = 0$ (1), 10 (2), 15 (3), and 30 (4).

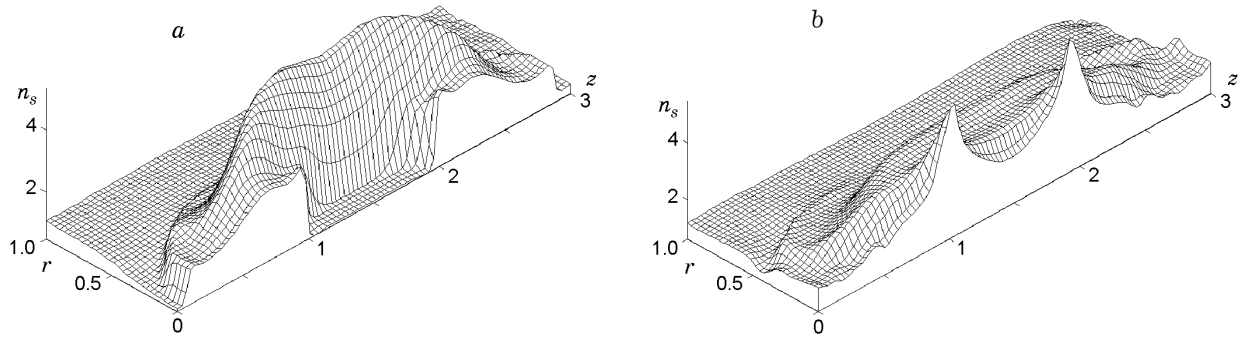

Fig. 8. Results of calculations with a heat source $Q_0 = 10^5$ (a) and $2 \cdot 10^5$ (b).

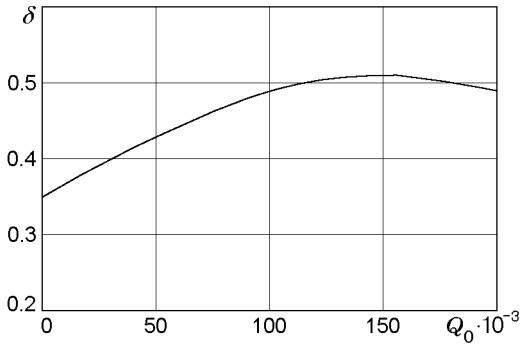

Fig. 9. Mean radius δ versus Q_0.

≈1.5, and ≈1.5 cm, respectively. Thus, the experiment also shows that the transverse expansion of the cloud is limited by the magnetic field. In the longitudinal direction, there is free gas-dynamic expansion of the plasma.

In the final series of calculations, we performed numerical simulation of plasma expansion in the presence of an extraneous heat source:

$$Q = \begin{cases} \tau n_s Q_0, & n_s \geqslant 1.5, \\ 0, & n_s < 1.5. \end{cases} \tag{23}$$

Formula (23) simulates the absorption of the relativistic electron beam energy by the plasma in the simplest approximation.

As follows from physical considerations, in the presence of an extraneous heat source, the gas-dynamic processes in the cloud should proceed at higher rate because the pressure gradient, and, hence, the gas-dynamic

force increase in this case. This is supported by the results of calculations with a heat source $Q_0 = 10^5$ presented in Fig. 8a (all calculations in this series were carried out on a 150×300 grid at $\Phi = 15$). As shown in Fig. 8a, in the calculation time, the perturbation reaches the boundaries of the calculation domain (cf. Fig. 5b). As the power of the heat source (i.e., Q_0) increases with increase in the temperature and pressure of the cloud during the calculation, the internal wave front stops and begins to move backward (Fig. 8b), filling the low-density region at the center with the plasma.

Figure 9 shows a curve of the mean radius of the cloud versus the power of the extraneous heat source at $t = 0.5$. The simplified model of the problem does not describe the heating of the ions of the gas cloud by the superthermal electrons of the background plasma, and, therefore, a general model is required to obtain detailed quantitative characteristics.

CONCLUSIONS

Thus, in the present paper, we proposed a mathematical model for describing the formation and expansion of a gas cloud that arose from a grain of lithium deuteride vaporized under the action of a relativistic electron beam.

The axisymmetric problem of the propagation of a dense plasma cloud into a rarefied background plasma in an external magnetic field with and without an external heat source is considered in a magnetohydrodynamic approximation using a simplified model.

The main regularities of the effect of the magnetic field on plasma expansion are obtained by numerical simulation. The effect of the external source on plasma expansion characteristics is estimated.

This work was carried out within the framework of the Federal Target Program "Integration" (Grant No. 274), the Program "Universities of Russia," and the Federal Target Scientific and Engineering Program "Research in the Priority Lines of Development of Civil Science and Engineering" [Grant No. 105-22/55(00)-P] and supported by the Russian Foundation for Fundamental Research (Grant Nos. 99-01-00619 and 99-07-90418).

REFERENCES

1. R. Yu. Akentjev, A. V. Arzhannikov, V. T. Arzhannikov, et al., "Experiments directed to creation of hot plasma with $\beta \sim 1$ at the GOL-3-II facility," in: 3rd Int. Conf. on Open Magnetic Systems for Plasma Confinement (Program and book of abstr.), Tsukuba Univ. (2000), p. 33.
2. V. T. Astrelin, A. V. Burdakov, and V. V. Postupaev, "Suppression of thermal conductivity and generation of ion-sound waves during plasma heating by an electron beam," *Fiz. Plazmy*, **24**, No. 5, 450–462 (1998).
3. A. V. Arzhannikobv, A. V. Burdakov, B. N. Breizman, et al., "Plasma heating by powerful relativistic electron beams," in: *Proc. VII Int. Conf. on Plasma Physics and Controlled Thermonuclear Fusion* (Innsbruck, 1978), Vol. 2, International Agency on Nuclear Power Engineering, Vienna (1979), pp. 623–627.
4. S. I. Braginskii, *Problems of Plasma Theory* [in Russian], Vol. 1, Atomizdat, Moscow (1963), pp. 191–195.
5. L. A. Artsimovich and R. Z. Sagdeev, *Plasma Physics for Physicists* [in Russian], Atomizdat, Moscow (1979), pp. 156–164.
6. V. M. Kovenya, "Splitting schemes in the finite-volume method," *Zh. Vychisl. Mat. Mat. Fiz.*, **41**, No. 1, 100–113 (2001).
7. V. M. Kovenya, G. A. Tarnavskii, and S. G. Chernyi, *Use of the Splitting Method in Aerodynamic Problems* [in Russian], Nauka, Novosibirsk (1990).
8. K. Longmire, *Elementary Plasma Physics*, Interscience Publ., New York (1963).